Research Square

Preprints are preliminary reports that have not undergone peer review.
They should not be considered conclusive, used to inform clinical practice,
or referenced by the media as validated information.

# Optical Semantic Holographic Communication

**Zhenming Yu**

yuzhenming@bupt.edu.cn

Beijing University of Posts and Telecommunications

**Xiangyong Dong**

Beijing University of Posts and Telecommunications

**Hongyu Huang**

Beijing University of Posts and Telecommunications

**Anxu Zhang**

China Telecom Research Institute, State Key Laboratory of Optical Fiber and Cable Manufacture Technology

**Yanlan Xiao**

University Of Electronic Science And Technology Of China

**Yan Ma**

Beijing University of Posts and Telecommunications

**Di Geng**

Beijing University of Posts and Telecommunications

**Wei Zhang**

Beijing University of Posts and Telecommunications

**Lipeng Feng**

China Telecom Research Institute, State Key Laboratory of Optical Fiber and Cable Manufacture Technology

**Xiaoli Huo**

China Telecom Research Institute, State Key Laboratory of Optical Fiber and Cable Manufacture Technology

**Daquan Yang**

Beijing University of Posts and Telecommunications

**Yue Zhou**

Beijing University of Posts and Telecommunications

**Xingyuan Xu**

Beijing University of Posts and Telecommunications https://orcid.org/0000-0002-8190-4700

**Peng Li**

Yangtze Optical Fiber and Cable Joint Stock Limited Company (YOFC)

**Qiang Guo**

Huawei Technologies Co.

**Huashun Wen**

https://orcid.org/0000-0003-0821-0072

**Heng Zhou**

University of Electronic Science and Technology of China https://orcid.org/0000-0002-5601-0772

**Junjie Li**

China Telecom Research Institute, State Key Laboratory of Optical Fiber and Cable Manufacture Technology

**Chengliang Zhang**

China Telecom Research Institute, State Key Laboratory of Optical Fiber and Cable Manufacture Technology

**David Moss**

swinburne university of technology https://orcid.org/0000-0001-5195-1744

**Kun Xu**

Beijing University of Posts and Telecommunications

---

**Article**

**Keywords:**

**Posted Date:** April 2nd, 2026

**DOI:** https://doi.org/10.21203/rs.3.rs-9091993/v1

**License:** This work is licensed under a Creative Commons Attribution 4.0 International License. Read Full License

**Additional Declarations:** There is **NO** Competing Interest.

---

## EDITORIAL NOTE:

23 April, 2026. Editorial Expression of Concern: This preprint includes images from the UVG-VPC dataset without citation or acknowledgement, contrary to the dataset's licensing requirements. The UVG-VPC dataset and its license terms are available at https://ultravideo.fi/UVG-VPC/index.html.

# Abstract

Holographic communication enables immersive metaverse interaction but transmitting dynamic media like point clouds demands unprecedented bandwidth, a key challenge for current networks. We propose an optical semantic holographic communication architecture integrating deep learning algorithms, coherence-cloned Kerr microcombs, and hollow-core optical fiber to meet bandwidth, fidelity, and low-latency requirements, achieving the first 100 km coherent transmission using coherence-cloned Kerr microcombs. Deep learning-enabled semantic joint coding-modulation (JCM) improves capacity by 65.3% and enhances channel robustness compared with conventional digital protocols. For phase-sensitive constellations of the JCM-generated discrete-time continuous-amplitude symbols, the microcombs act as phase-matched carriers/oscillators for stable coherent detection. The ultra-low nonlinearity of the hollow-core fiber preserves semantic integrity, further suppresses link-phase noise, and synergizes with microcombs for physical-layer phase noise control. Our system achieves 2.5875 trillion 3D points/s with superior quality, setting a new artificial intelligence-native metaverse benchmark.


# Introduction

Holographic communication, which enables real-time three-dimensional (3D) interaction between remote users, is a foundational pillar of the emerging metaverse[1–3]. However, delivering high-fidelity holographic experiences based on point clouds (PCs), virtual reality, and augmented reality requires unprecedented data transmission capacity[4, 5]. Of these experiences, PCs, in which objects are represented as unordered sets of 3D points, best exemplify the extreme bandwidth demands of holographic media. For instance, a single depth camera that captures 30 frames per second generates 2.06 gigabits of raw data per second for a single view. High-fidelity applications often require multi-angle recordings from dozens of synchronized cameras, allowing them to produce hundreds of gigabits or even terabits of data per second per holographic channel[6–8]. This data rate surpasses the throughput of conventional two-dimensional (2D) media by several orders of magnitude, imposing a critical burden on network capacity. Notably, fiber optic communication systems can support terabit-per-second and even petabit-per-second data rates, offering the most viable solution for meeting the high demands of holographic communication[9–15]. However, conventional fiber-based transmission architectures depend nearly exclusively on the standard single-mode fiber (SSMF), which suffers from inherent physical limitations. Kerr nonlinearity and chromatic dispersion in SSMFs intensify with transmission distance and input power, distorting the quality of holographic PC signals. Meanwhile, phase noise accumulation and high latency degrade the optical carrier coherence in SSMFs, further eroding PC reconstruction fidelity. These drawbacks often force reliance on complex and latency-heavy digital signal processing (DSP) algorithms for mitigation, which ultimately undermines the real-time interaction of holographic communication. Thus, while fiber provides sufficient bandwidth, identifying the best method for enabling the fiber's capacity to facilitate holographic media remains a critical unsolved challenge.

In this work, we introduce an optical semantic holographic communication architecture. This architecture is empowered by deep learning (DL), microcombs, and hollow-core fiber (HCF) to meet the

requisite bandwidth, fidelity, and low-latency requirements, as shown in Fig. 1. Leveraging advancements in semantic-aware communication, our DL-driven framework prioritizes the transmission of meaningful 3D features over raw PC bit streams[16–19]. At the core of our system is a 3D convolutional neural network designed for the JCM protocol. This neural network generates discrete-time continuous-amplitude (DTCA) semantic samples that outperform conventional digital data transmission methods (e.g., bit-based PC compression, low-density parity-check (LDPC))[20–22] by boosting transmission capacity by 65.3%, thereby enhancing the quality of the received holograms and the resilience to channel impairments. Moreover, our system employs coherence-cloned Kerr microcombs—produced in photonic-integrated microcavities—as carriers and local oscillators to facilitate wavelength division multiplexing (WDM) holographic transmission[23–26]. By synchronizing the transmitter and receiver microcombs via a two-point locking strategy[27, 28], we achieved ultrahigh mutual phase coherence among 15 WDM channels, effectively resolving the phase noise originating from independent laser sources and laying the groundwork for stable detection of the irregular DTCA signal constellations.

To establish a framework for inherently robust high-performance signal propagation, an advanced physical transmission medium is required. SSMFs, however, are hindered by severe Kerr nonlinearity, which inherently limits their tolerance to high launched optical power (LOP)—a critical constraint for extending transmission reach, as higher LOP is needed to mitigate signal attenuation over long distance[29]. Furthermore, the high nonlinearity of SSMF further induces link-level phase noise when LOP is increased, exacerbating DTCA signal distortion and coherence degradation with increased transmission distance. SSMF also suffers from large chromatic dispersion, compounding these transmission impairments. In contrast, HCFs exhibit ultra-low Kerr nonlinearity, enabling them to tolerate significantly higher LOP than SSMFs. This high LOP capability supports longer transmission reach by mitigating signal attenuation and suppresses the nonlinearity-induced link-level phase noise that corrupts DTCA constellations in SSMFs[30, 31]. Concurrently, HCFs feature minimal chromatic dispersion, eliminating the need for latency-intensive dispersion compensation modules[32–34]. This is a critical advantage over SSMF-based systems, in which dispersion compensation modules add a substantial DSP delay that conflicts with the low-latency demands of holographic transmission. Additionally, HCFs' suppression of LOP-related link-originated phase noise works in tandem with the microcombs' laser source phase stabilization. Together, they suppress all major phase noise sources across the transmission chain and further secure DTCA signal integrity.

By integrating DL-driven semantic encoding, phase-locked coherence-cloned microcombs, and low-impairment HCFs, we demonstrate a notable advance in high-capacity optical holographic communication and realize 100 km coherent transmission enabled by the two-point locking of coherence-cloned Kerr microcombs for the first time. This integrated system achieves a transmission rate of 2.5875 trillion 3D points/s, with no need for complex digital algorithms (e.g., dispersion compensation or carrier phase recovery)[35, 36]. Our approach offers promising solutions for real-time high-capacity holographic data transmission, accelerating the development of a wide range of applications—from robotics to the metaverse.

# Results

**DL-enabled semantic–holographic–optic communication: A new concept.** As a pivotal building block of our system, semantic communication represents a paradigm shift in the basic principles of communication. This shift prioritizes the conveyance of meaningful information rather than raw data bits. Unlike traditional systems, which focus on bit-level accuracy, semantic communication involves the extraction and transmission of essential semantic features (e.g., contextual or task-relevant data), thereby significantly reducing bandwidth requirements while maintaining utility. This may be particularly revolutionary for data-intensive applications, such as holographic interactions, whose raw data volumes can overwhelm host networks. Moreover, advances in semantic communication are supported largely by the rapid evolution of DL models, such as convolutional neural networks, transformers, and recurrent neural networks, which excel at extracting semantic features from raw data and coding them, thus enabling context-aware transmission. DL can also facilitate joint source–channel coding, in which compression and error correction are merged into a unified neural architecture. While it violates the strict Shannon separation theorem, joint source–channel coding often outperforms separate source and channel coding in dynamic, real-world scenarios[37–40].

The core innovation of the semantic encoder is its 3D convolution-based JCM network[41, 42], designed to facilitate the semantic transmission of PCs, as shown in Fig. 2. The JCM network uses multiscale 3D convolutional blocks to effectively capture spatial information across multiple scales, which is then aggregated to enhance spatial correlations and optimize coding performance[43–45]. Large convolutional kernels in the JCM network capture architectural features, while small convolutional kernels extract fine-grained details. These kernels work in tandem to efficiently extract and encode semantic information. All the parameters of this network are described in the Supplementary Materials. Initially, the PC is partitioned into discrete blocks that are sequentially processed for encoding by the network. During encoding, 3D convolution operations extract spatial features from the PC blocks while compressing redundant data[46, 47]. These features are then encoded into channel symbols, reshaped into 2D IQ signals, and transmitted through an optical fiber. In the receiver, the transmitted signals are reconstructed into PC blocks by a joint decoding and demodulation (JDD) network, which performs the inverse operation of the JCM network. The 3D deconvolution operations within the JDD network decompress the data and restore the extracted features. Finally, the PC blocks are merged to reconstruct the original PC.

To assess our method's performance, we implement a conventional optical transmission system framework following digital communication protocols, thereby establishing a comparative baseline for evaluating the model's efficacy. For source coding, octree-based geometric point cloud compression coding is used. The channel coding incorporates soft-decision LDPC codes with a code rate of 3/4[22, 48]. The modulation schemes—quadrature phase shift keying (QPSK) and 16-quadrature amplitude modulation (16-QAM)—are selected to match the prevailing channel conditions.

The outputs of the JCM network are DTCA symbols. First, the JCM jointly optimizes source compression and channel transmission using DL models. This is performed in a continuous space using gradient

descent algorithms, which naturally produce encoder outputs with a continuous amplitude. The encoder neural network consists of a series of convolution operations and activation functions that enable nonlinear transformation of the PC's spatial features. The output symbols exhibit a continuous amplitude because this process does not involve bit-symbol quantization mapping. Moreover, according to Shannon's theorem, when the signal-to-noise ratio (SNR) of an additive white Gaussian noise channel is limited, a Gaussian-distributed continuous-amplitude input can approach the maximum channel capacity[49]. Considering that JCM is designed to approximate this theoretical limit, it inherently tends to generate symbols with continuous amplitudes that follow a Gaussian distribution. Unlike canonical digital signal formats (e.g., QPSK, 16-QAM), DTCA symbols have entirely irregular constellations, making it difficult to track phase noise between the independent signal carrier and the local oscillator[27, 50].

To address this challenge, we employ two advanced photonic technologies, namely coherence-cloned Kerr microcombs and HCFs, as shown in Fig. 2. The cloned microcombs function as both laser carriers and local oscillators, ensuring coherent transmission. During transmission, pump and pilot signals are delivered to the receiver to regenerate the optical combs. This facilitates two-point locking between the regenerated and transmitted combs, enabling self-homodyne detection. This configuration significantly mitigates signal phase noise induced by the laser source. Additionally, HCFs effectively suppress phase noise introduced during optical fiber transmission, ensuring that the performance advantages of DTCA symbols (with their irregular constellations) and microcomb-enabled coherent detection are fully exploited. SSMFs are not favorable because they impose three fundamental constraints in holographic transmission. First, severe Kerr nonlinearity inherently limits their tolerance to high LOP—a critical barrier for extending transmission distance, considering that higher LOP is required to mitigate attenuation over long distances. Second, this high nonlinearity, when combined with even moderately increased LOP, induces significant link-phase noise that microcombs cannot mitigate, necessitating complex carrier phase-recovery algorithms. Third, substantial chromatic dispersion degrades signal integrity as the transmission distance increases, further limiting their reach. In contrast, HCFs exhibit ultra-low Kerr nonlinearity and can tolerate significantly higher LOP, supporting 100 km transmission by mitigating attenuation. This low nonlinearity also suppresses LOP-induced link-phase noise, eliminating the need for carrier phase recovery. Concurrently, their minimal chromatic dispersion avoids distance-related distortion without dispersion compensation.

The high-capacity holographic semantic transmission empowered by advanced photonics obviates complex, latency-heavy DSP algorithms. By integrating JCM-based semantic encoding with microcombs' two-point-locked coherent detection and HCFs' high-LOP tolerance, our system achieves the stable transmission of 2.5875 trillion 3D points/s over 100 km without complex DSP for the first time. This breakthrough not only meets holographic communication's high-fidelity and real-time demands but also unlocks long-haul capabilities for semantic holography, enabling practical applications in robotics and the metaverse.

**Coherent transmission enabled by HCFs and the coherence-cloned regeneration of dissipative Kerr soliton microcombs.** In the experiment, two silicon nitride ($Si_3N_4$) on-chip microring cavities with a free

spectral range of 100 GHz are employed to generate mutually coherent dual microcombs, as depicted in Fig. 3(a). The auxiliary laser heating method is used to generate dissipative Kerr soliton (DKS) microcombs in two silicon-integrated microcavities[51, 52]. On the transmitter side, a DKS microcomb is generated, from which 15 comb lines are selected as the data carriers and modulated using a commercial IQ modulator. As shown in Fig. 3(a), the 15-channel signals and pump laser are transmitted 100 km to the receiver via a 10-segment HCF.

On the receiver side, the transmitted pump laser is used to regenerate another soliton microcomb, which acts as the receiver local oscillator microcomb (see Fig. 3(b)). At this stage, the transmitter carrier microcomb and the receiver local oscillator microcomb share the same pump laser[28, 53]. Furthermore, we extract the 14th comb line of the laser carrier microcomb as a pilot signal, which is phase-locked to the corresponding receiver comb line using an optical phase-locked loop. With this approach, the transmitter comb and receiver comb are two-point locked with faithfully cloned frequency stability and phase coherence[28]. As shown in Fig. 3(c), after two-point locking, the beat note linewidth between the $14^{th}$ transmitter comb and the receiver comb is significantly suppressed compared with that before locking, which facilitates efficient coherent detection of the DTCA symbols[28, 45].

Moreover, the characteristics of the HCF used in our experiment are detailed in Fig. 3(d)–(f). Fig. 3(d) shows a cross-sectional electron microscope image, revealing a double-nested antiresonant nodeless architecture with three capillary sizes: 30.8 μm (large), 22.5 μm (medium), and 8.8 μm (small), with membrane thicknesses of 1.12, 1.15, and 1.18 μm, respectively. The central core diameter is 29.8 μm, and the average gap between nested tubes is 5.1 μm, with dimensional deviations < 5% to ensure manufacturing uniformity. Fig. 3(e) presents the HCF's attenuation spectrum (resolution = 0.002 nm), demonstrating an average attenuation of ~0.185 dB/km, superior to conventional G.652 SSMFs. Fig. 3(f) shows the latency results; the HCF exhibits 3.37 μs/km, a ~32.3% reduction compared with the SSMF (4.98 μs/km). This advantage originates from the hollow core, which enables faster light propagation[54, 55].

**Holographic data transmission performance.** Using coherence-cloned microcombs, we developed a 15-channel, 30-Gbaud, single-polarization holographic data 100 km HCF transmission system. PC transmission performance was evaluated based on the point-to-point peak SNR (PSNR) between the received and transmitted PCs[56]. Fig. 4(a) illustrates the transmission results for all 15 channels, demonstrating the effectiveness of the proposed system. For 16-QAM transmission, the bit error rates (BERs) before LDPC decoding for all channels are below . After LDPC decoding, all channels achieve error-free transmission. At the same transmission rate, semantic transmission improves the PC transmission's PSNR by approximately 5 dB. The visual results, shown in Fig. 4(b), demonstrate that the semantic transmission scheme significantly enhances the transmission quality. By simultaneously using multiple parallel channels, the transmission system enables the transmission of 2.5875 trillion 3D points (i.e., individual points that make up a PC) per second.

Next, we evaluate the optical power budget for coherent detection and examine the relationship between the calculated PSNR score and the received optical power (ROP) for both traditional digital communication and semantic communication in channel C32. The results are shown in Fig. 4(c). When the ROP falls below −25 dBm, the system can no longer support error-free 16-QAM transmission and requires the use of QPSK modulation. However, QPSK modulation reduces the system's bit rate. To maintain the same PC transmission rate, the compression ratio of the source coding (GPCC) must be increased. As a result, the PC transmission quality enabled by traditional digital communication schemes significantly deteriorates in the low ROP region. In contrast, the semantic communication scheme maintains high PC transmission quality even when the ROP is as low as −31 dBm. The improvement in PSNR can reach approximately 5 and 8 dB compared with the 16-QAM and QPSK schemes, respectively. Visualizations of the PC transmission results for both the semantic and QPSK schemes when the ROP is −31 dBm are shown in Fig. 4(d). Under the condition of poor channel performance, the semantic scheme continues to enable excellent transmission performance, and it significantly outperforms the traditional digital scheme in terms of visual quality.

Then, we investigate the relationship between the calculated PSNR score and the LOP for both traditional digital communication and semantic communication in channel C32. The experimental results are compiled in Fig. 4(e). When sweeping LOP from 20 to 30 dBm for 100 km HCF transmission, the semantic communication scheme maintains a consistently high PSNR of ~73.3 dB. In contrast, traditional 16-QAM and QPSK schemes exhibit stagnant performance at ~68.3 and ~65.3 dB, respectively. Visual comparisons of the PC transmission results between the semantic scheme and 16-QAM at 30 dBm LOP are presented in Fig. 4(f). These experimental results clearly demonstrate that HCF introduces no PSNR penalty, even at 30 dBm LOP. This directly confirms HCF's negligible nonlinearity, which is required to achieve longer transmission distances using microcomb-based holographic communication. Furthermore, leveraging the HCF's inherent minimal chromatic dispersion and ultra-low Kerr nonlinearity simplifies the holographic communication receiver architecture, eliminating the need for complex, latency-intensive DSP modules, such as dispersion compensation and nonlinearity compensation. This provides a foundational framework for low-latency holographic transmission.

Our system supports 30-Gbaud 16-QAM 100 km HCF transmission across 15 channels, achieving an aggregate bit rate of 1.8 Tb/s. After accounting for a 25% forward error correction overhead, the net bit rate reaches 1.35 Tb/s. As demonstrated in Fig. 5(a), the combination of two-point locking and HCF's ultra-low nonlinearity significantly suppresses phase noise, ensuring high transmission quality. As shown in Fig. 5(b), adjusting the source coding compression ratio reveals a trade-off between transmission quality and point cloud (PC) transmission rate. In contrast, the semantic communication scheme achieves both high transmission efficiency and superior quality simultaneously. Even when the communication rate is boosted by 65.3%, this scheme can still attain about 1.2 dB improvement in PSNR. Moreover, at comparable transmission speeds, the semantic scheme exhibits markedly better performance—a conclusion corroborated by Fig. 5(c), which visually compares the performance of the semantic scheme against that of the conventional 16QAM transmission scheme across different transmission rates.

# Discussion

This work introduces an optical semantic holographic communication architecture empowered by DL, microcombs, and HCFs to address the bandwidth and low-latency requirements of high-fidelity PC data. We demonstrate a semantic-aware JCM network that effectively encodes and decodes 3D PCs, achieving a 65.3% capacity gain over traditional digital protocols while enhancing reconstruction quality through context-aware feature prioritization. To resolve the irregular constellation distribution of the semantic DTCA symbols generated by our JCM neural network, we deploy coherence-cloned Kerr microcombs as phase-matched carriers and local oscillators in a 15-channel WDM system—laying the groundwork for stable coherent detection of non-canonical signal formats. In addition, HCFs are employed to address the remaining link-level barriers: their ultra-low Kerr nonlinearity suppresses LOP-induced phase noise, minimal chromatic dispersion avoids distance-induced distortion, and high LOP tolerance supports 100 km communication by mitigating attenuation. This tripartite synergy eliminates the need for conventional phase-recovery and dispersion-correction DSP algorithms, ensuring robust detection of holographic semantic signals. Demonstrating a record transmission rate of 2.5875 trillion 3D points/s, our system achieves unprecedented scalability for holographic media, effectively overcoming practical network constraints and meeting the demand for terabit-per-second data rates. By unifying DL-driven semantic compression with ultra-low-noise photonics, this work establishes a foundational framework for high-capacity, low-latency holographic communication in the era of artificial intelligence and the metaverse.

# Methods

**A novel semantic encoding network.** Fig. S1 and Table S1 in the Supplementary Materials present the detailed architecture of our proposed semantic encoding network. Three-dimensional (3D) convolution serves as the core of this network. In the encoder, a 3D convolution layer with a stride of two downsamples point cloud (PC) blocks. Features are extracted from the PC blocks, and the blocks are compressed, by concatenating three 3D downsampling convolution layers and two dual-channel 3D convolution blocks. In the network, the combination of large- and small-scale convolutions effectively captures and encodes both the architectural structure and the fine details of the PC. The dual-channel 3D convolutional blocks map features onto different high-dimensional spaces, facilitating the compression of redundant information. The decoding network adopts a structure that inverts the structure of the encoding network. The former network consists of three successive 3D upsampling deconvolution layers and two dual-channel 3D deconvolution blocks. These components work together to decompress features and reconstruct PC blocks. The three 3D upsampling deconvolution layers progressively restore spatial resolution by expanding the dimensions of the compressed features, while the two dual-channel 3D deconvolution blocks enhance feature reconstruction capability by mapping features onto different high-dimensional spaces. This architecture ensures that the reconstructed PC blocks maintain spatial fidelity and structural integrity, effectively reversing the compression process applied during encoding.

**Digital signal processing procedure.** Fig. S3 in the Supplementary Materials provides a diagram illustrating the digital signal processing streams. On the transmitter side, in the semantic communication scheme, the input PCs are encoded into channel symbols using joint coding and modulation (JCM). In the digital communication scheme, GPCC encoding compresses the information into bits, while LDPC encoding introduces redundancy to correct bit errors during transmission. The encoded bits are then mapped to channel symbols using quadrature phase shift keying or 16-quadrature amplitude modulation to facilitate transmission. These symbols are upsampled and pulse-shaped using a square root raised cosine (SRRC) filter with a 0.1 roll-off factor. The signals are subsequently resampled to match the 60 GSa/s sampling rate of the AWG. On the receiver side, the signals are first resampled to two samples per symbol. IQ imbalances in the received signal are corrected using Gram–Schmidt orthogonalization. The SRRC filter is used as a matched filter. A 41-tap linear equalizer is employed to compensate for the channel response. The frequency offset is estimated using a standard fourth-power fast Fourier transform. Carrier phase compensation is not required due to self-homodyne detection, and the recovered symbols are obtained. In the semantic communication scheme, joint demodulation and decoding (JDD) reconstructs the symbols into the original PC. In the digital communication scheme, soft-decision LDPC decoding is applied to convert the recovered symbols into corrected bits, which are then decoded via GPCC to reconstruct the PC.

### Data and Materials Availability

The data that support the findings of this study and custom codes are available from the corresponding author upon reasonable request.

## Declarations


### Acknowledgments

This work was financially supported by the National Key R&D Program of China (No.2023YFB2905900); National Natural Science Foundation of China (No. 62522502, 62371056); Major Science and Technology Support Program of Hebei Province (No. 252X1701D); Sponsored by Beijing Nova Program; Shenzhen Science and Technology Program (KJZD20230923115202006); the Fund of State Key Laboratory of Information Photonics and Optical Communication BUPT (No. IPOC2025ZZ02); the Fundamental Research Funds for the Central Universities (No. 530424001, 2024ZCJH13).


### Author Contributions

Z.Y., X.D., H.H., H.Z., and K.X. conceptualized and designed the optical semantic holographic communication architecture. D.G., Y.M., W.Z., and Q.G. designed the 3D convolution-based PC JCM and JDD network. X.D., H.H., Y.X., A.Z., and P.L. constructed coherent transmission experiments based on coherence-cloned regeneration of DKS microcombs and hollow-core fiber. L.F., X.H., D.Y., H.W., and Y.Z. analyzed the coherent holographic transmission results enabled by deep learning, clone combs and

hollow-core fiber. Z.Y., X.D., Y.X., H.Z., X.X, J.L., C.Z. and D.J.M. prepared the figures and wrote the manuscript, with contributions from all other authors. Z.Y., A.Z., H.Z., and K.X. supervised the project.

## References


1. Wang, Y. *et al.* A Survey on Metaverse: Fundamentals, Security, and Privacy. *IEEE Commun. Surv. Tutor.* **25**, 319–352 (2023).
2. Yu, H. *et al.* Deep learning-based incoherent holographic camera enabling acquisition of real-world holograms for holographic streaming system. *Nat. Commun.* **14**, 3534 (2023).
3. Shi, L., Li, B., Kim, C., Kellnhofer, P. & Matusik, W. Towards real-time photorealistic 3D holography with deep neural networks. *Nature* **591**, 234–239 (2021).
4. El Essaili, A. *et al.* Holographic communication in 5G networks. *Ericsson Technol. Rev.* **2022**, 2–11 (2022).
5. Liu, Z. *et al.* Point Cloud Video Streaming: Challenges and Solutions. *IEEE Netw.* **35**, 202–209 (2021).
6. HOLOGRAPHIC-TYPE COMMUNICATION: A NEW CHALLENGE FOR THE NEXT DECADE. **3**, (2022).
7. Huang, Y. *et al.* Toward Holographic Video Communications: A Promising AI-Driven Solution. *IEEE Commun. Mag.* **60**, 82–88 (2022).
8. Bian, C., Shao, Y. & Gündüz, D. Wireless Point Cloud Transmission. in *2024 IEEE 25th International Workshop on Signal Processing Advances in Wireless Communications (SPAWC)* 851–855 (2024). doi:10.1109/SPAWC60668.2024.10694621.
9. Liu, J. *et al.* 1-Pbps orbital angular momentum fibre-optic transmission. *Light Sci. Appl.* **11**, 202 (2022).
10. Matsushita, A., Nakamura, M., Yamamoto, S., Hamaoka, F. & Kisaka, Y. 41-Tbps C-Band WDM Transmission With 10-bps/Hz Spectral Efficiency Using 1-Tbps/λ Signals. *J. Light. Technol.* **38**, 2905–2911 (2020).
11. Almonacil, S. *et al.* C-band unrepeated transmission system over 291-km at net throughput of 41.3-Tbps without ROPA. in *49th European Conference on Optical Communications (ECOC 2023)* vol. 2023 609–612 (2023).
12. Ozaki, J. *et al.* C+L-band InP-based Coherent Driver Modulator Enabled Net-1.8 Tbps/λ Transmission. *J. Light. Technol.* 1–7 (2024) doi:10.1109/JLT.2024.3453510.
13. Carbó Meseguer, A. *et al.* On the Road to 1-Pbps systems: Experimental Demonstration of an Energy Efficient 500-Tbps Transatlantic Cable with 200-μm Outer Diameter Fibers. in *2023 Optical Fiber Communications Conference and Exhibition (OFC)* 1–3 (2023). doi:10.1364/OFC.2023.Tu2G.5.
14. Rademacher, G. *et al.* Peta-bit-per-second optical communications system using a standard cladding diameter 15-mode fiber. *Nat. Commun.* **12**, 4238 (2021).
15. Rashidinejad, A., Nguyen, A., Olson, M., Hand, S. & Welch, D. Real-Time Demonstration of 2.4Tbps (200Gbps/λ) Bidirectional Coherent DWDM-PON Enabled by Coherent Nyquist Subcarriers. in *2020 Optical Fiber Communications Conference and Exhibition (OFC)* 1–3 (2020).

16. Liu, X., Liang, H., Bao, Z., Dong, C. & Xu, X. A Semantic Communication System for Point Cloud. *IEEE Trans. Veh. Technol.* 1–17 (2024) doi:10.1109/TVT.2024.3456099.
17. Zhang, W. *et al.* Lightweight Joint Coding-Modulation Optical Fiber Communication System for Point Cloud. *IEEE Trans. Commun.* 1–1 (2024) doi:10.1109/TCOMM.2024.3455233.
18. Lu, K. *et al.* Rethinking Modern Communication from Semantic Coding to Semantic Communication. *IEEE Wirel. Commun.* **30**, 158–164 (2023).
19. Luo, X., Chen, H.-H. & Guo, Q. Semantic Communications: Overview, Open Issues, and Future Research Directions. *IEEE Wirel. Commun.* **29**, 210–219 (2022).
20. Schwarz, S. *et al.* Emerging MPEG Standards for Point Cloud Compression. *IEEE J. Emerg. Sel. Top. Circuits Syst.* **9**, 133–148 (2019).
21. Gallager, R. Low-density parity-check codes. *IRE Trans. Inf. Theory* **8**, 21–28 (1962).
22. Cushon, K., Larsson-Edefors, P. & Andrekson, P. Low-Power 400-Gbps Soft-Decision LDPC FEC for Optical Transport Networks. *J. Light. Technol.* **34**, 4304–4311 (2016).
23. Corcoran, B. *et al.* Ultra-dense optical data transmission over standard fibre with a single chip source. *Nat. Commun.* **11**, 2568 (2020).
24. Chang, L., Liu, S. & Bowers, J. E. Integrated optical frequency comb technologies. *Nat. Photonics* **16**, 95–108 (2022).
25. Pfeifle, J. *et al.* Coherent terabit communications with microresonator Kerr frequency combs. *Nat. Photonics* **8**, 375–380 (2014).
26. Zhang, C. *et al.* High-fidelity sub-petabit-per-second self-homodyne fronthaul using broadband electro-optic combs. *Nat. Commun.* **15**, 6621 (2024).
27. Zhang, C. *et al.* Clone-comb-enabled high-capacity digital-analogue fronthaul with high-order modulation formats. *Nat. Photonics* **17**, 1000–1008 (2023).
28. Geng, Y. *et al.* Coherent optical communications using coherence-cloned Kerr soliton microcombs. *Nat. Commun.* **13**, 1070 (2022).
29. Amari, A. *et al.* A Survey on Fiber Nonlinearity Compensation for 400 Gb/s and Beyond Optical Communication Systems. *IEEE Commun. Surv. Tutor.* **19**, 3097–3113 (2017).
30. Liu, Z. *et al.* Nonlinearity-Free Coherent Transmission in Hollow-Core Antiresonant Fiber. *J. Light. Technol.* **37**, 909–916 (2019).
31. Hong, Y. *et al.* Beyond Terabit/s/λ Nonlinearity-Free Transmission Over the Hollow-Core Fiber. *J. Light. Technol.* **43**, 6306–6312 (2025).
32. Numkam Fokoua, E., Abokhamis Mousavi, S., Jasion, G. T., Richardson, D. J. & Poletti, F. Loss in hollow-core optical fibers: mechanisms, scaling rules, and limits. *Adv. Opt. Photonics* **15**, 1 (2023).
33. Petrovich, M. *et al.* Broadband optical fibre with an attenuation lower than 0.1 decibel per kilometre. *Nat. Photonics* **19**, 1203–1208 (2025).
34. Poggiolini, P. & Poletti, F. Opportunities and Challenges for Long-Distance Transmission in Hollow-Core Fibres. *J. Light. Technol.* **40**, 1605–1616 (2022).

35. Savory, S. J. Digital Coherent Optical Receivers: Algorithms and Subsystems. *IEEE J. Sel. Top. Quantum Electron.* **16**, 1164–1179 (2010).
36. Zafra, S. O., Pang, X., Jacobsen, G., Popov, S. & Sergeyev, S. Phase noise tolerance study in coherent optical circular QAM transmissions with Viterbi-Viterbi carrier phase estimation. *Opt. Express* **22**, 30579 (2014).
37. Niu, K. *et al.* A Paradigm Shift toward Semantic Communications. *IEEE Commun. Mag.* **60**, 113–119 (2022).
38. Guo, S. *et al.* A Survey on Semantic Communication Networks: Architecture, Security, and Privacy. *IEEE Commun. Surv. Tutor.* 1–1 (2024) doi:10.1109/COMST.2024.3516819.
39. Dai, J. *et al.* Communication Beyond Transmitting Bits: Semantics-Guided Source and Channel Coding. *IEEE Wirel. Commun.* **30**, 170–177 (2023).
40. Chaccour, C., Saad, W., Debbah, M., Han, Z. & Poor, H. V. Less Data, More Knowledge: Building Next Generation Semantic Communication Networks. *IEEE Commun. Surv. Tutor.* 1–1 (2024) doi:10.1109/COMST.2024.3412852.
41. Huang, H. *et al.* Optical Fiber Communication System Based on Intelligent Joint Source-Channel Coded Modulation. *J. Light. Technol.* **42**, 2009–2017 (2024).
42. Mu, Y. *et al.* Low-Resolution Joint Encoding-Modulation Optical Fiber Communication System. *J. Light. Technol.* 1–10 (2024) doi:10.1109/JLT.2024.3486561.
43. Tran, D., Bourdev, L., Fergus, R., Torresani, L. & Paluri, M. Learning Spatiotemporal Features with 3D Convolutional Networks. in *2015 IEEE International Conference on Computer Vision (ICCV)* 4489–4497 (IEEE, Santiago, Chile, 2015). doi:10.1109/ICCV.2015.510.
44. Fu, F. *et al.* Rapid vessel segmentation and reconstruction of head and neck angiograms using 3D convolutional neural network. *Nat. Commun.* **11**, 4829 (2020).
45. Lee, J., Lee, H. & Mun, D. 3D convolutional neural network for machining feature recognition with gradient-based visual explanations from 3D CAD models. *Sci. Rep.* **12**, 14864 (2022).
46. Alexiou, E., Tung, K. & Ebrahimi, T. Towards neural network approaches for point cloud compression. in *Applications of Digital Image Processing XLIII* (eds Tescher, A. G. & Ebrahimi, T.) 4 (SPIE, Online Only, United States, 2020). doi:10.1117/12.2569115.
47. Guarda, A. F. R. *et al.* Deep Learning-Based Point Cloud Coding and Super-Resolution: a Joint Geometry and Color Approach. *IEEE Trans. Multimed.* 1–13 (2023) doi:10.1109/TMM.2023.3338081.
48. Jose, R. & Pe, A. Analysis of hard decision and soft decision decoding algorithms of LDPC codes in AWGN. in *2015 IEEE International Advance Computing Conference (IACC)* 430–435 (2015). doi:10.1109/IADCC.2015.7154744.
49. Shannon, C. E. A mathematical theory of communication. *Bell Syst. Tech. J.* **27**, 379–423 (1948).
50. Huang, H. *et al.* Integrated Coherent Optical Fiber Communication System with Discrete-Time Analog Transmission. in *Optical Fiber Communication Conference (OFC) 2024* Th2A.32 (Optica Publishing Group, San Diego California, 2024). doi:10.1364/OFC.2024.Th2A.32.

51. Xiao, Y. *et al.* Optimizing auxiliary laser heating for Kerr soliton microcomb generation. *Opt. Lett.* **49**, 1129 (2024).
52. Zhou, H. *et al.* Soliton bursts and deterministic dissipative Kerr soliton generation in auxiliary-assisted microcavities. *Light Sci. Appl.* **8**, 50 (2019).
53. Geng, Y. *et al.* Phase noise of Kerr soliton dual microcombs. *Opt. Lett.* **47**, 4838 (2022).
54. Feng, L. *et al.* Enabling 1200-km optical DNANF transmissions via the space–time coded digital subcarrier modulation. *Opt. Lett.* **50**, 4170 (2025).
55. Feng, L. *et al.* Demonstration of Single-span 100km Hollow Core Fiber Bidirectional Transmission with 1Tb/s/λ Real-time Signals. *Opt. Fiber Commun. Conf.* (2025).
56. Tian, D., Ochimizu, H., Feng, C., Cohen, R. & Vetro, A. Geometric distortion metrics for point cloud compression. in *2017 IEEE International Conference on Image Processing (ICIP)* 3460–3464 (2017). doi:10.1109/ICIP.2017.8296925.
57. Wang, J., Zhu, H., Liu, H. & Ma, Z. Lossy Point Cloud Geometry Compression via End-to-End Learning. *IEEE Trans. Circuits Syst. Video Technol.* **31**, 4909–4923 (2021).

# Figures

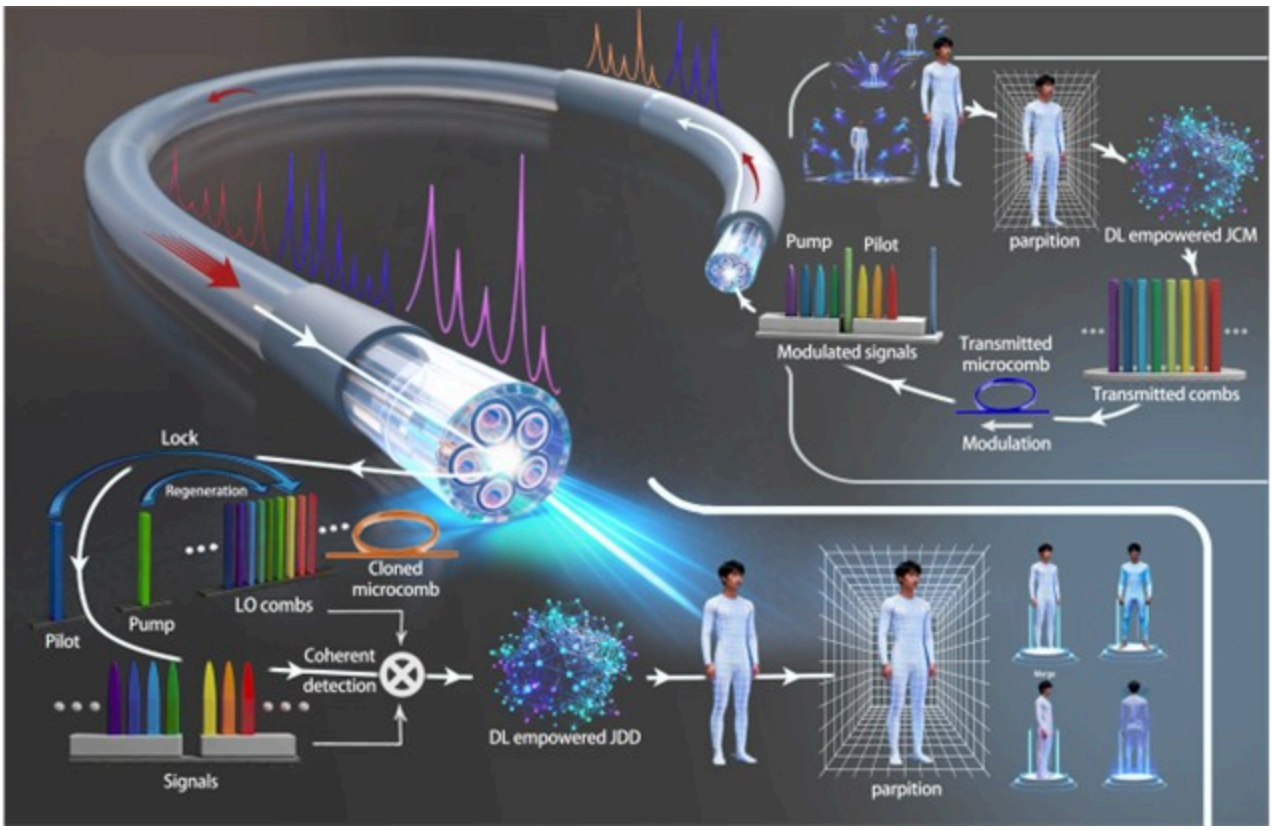



**Figure 1**

**The optical semantic holographic communication architecture.** Input PCs are partitioned, semantically compressed into continuous-amplitude DTCA symbols by a 3D convolution-based JCM network,

reshaped into signals, and transmitted via HCF. At the receiver, coherence-cloned microcombs (regenerated via pump signals and phase-locked via pilot signals for self-homodyne detection) and a JDD network reconstruct the original PCs. HCF's ultra-low nonlinearity and chromatic dispersion overcome SSMF's inherent limitations, enabling high-capacity, long-haul holographic transmission without complex DSP.

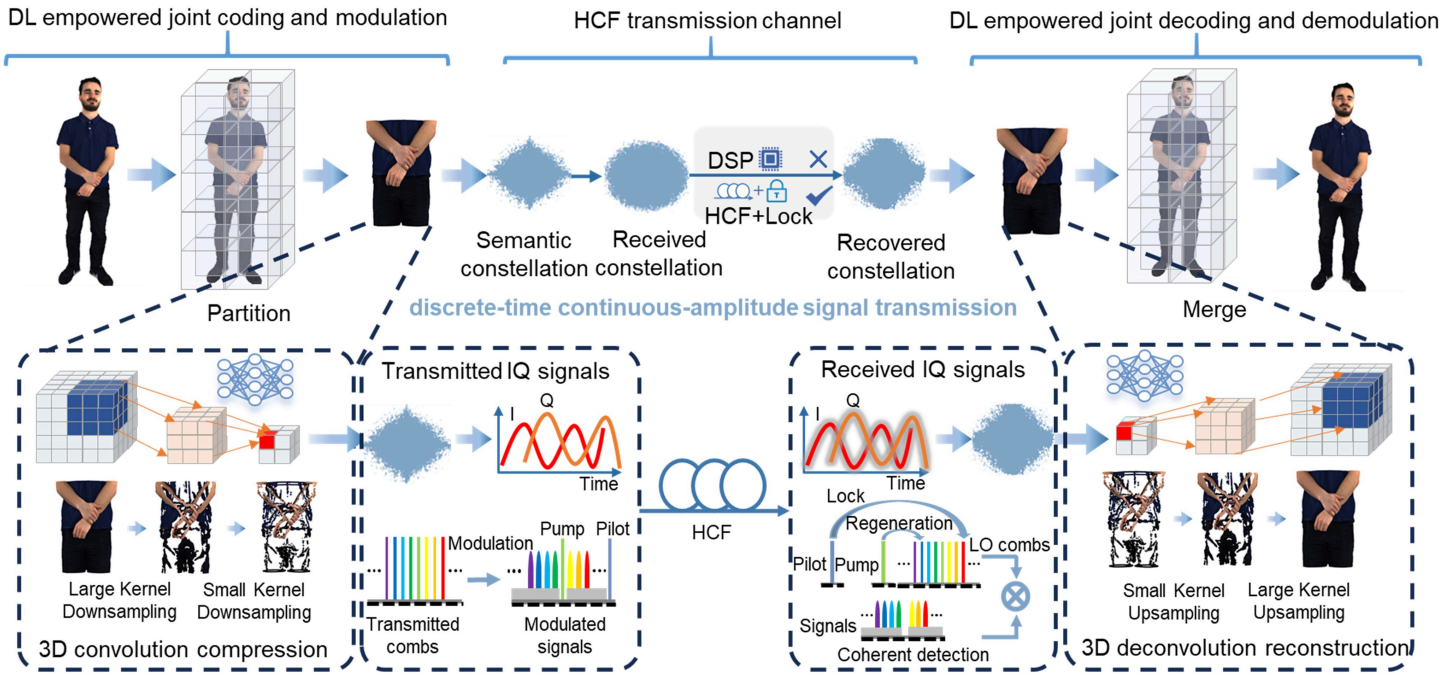



**Figure 2**

**JCM/JDD network workflow for HCF-based holographic semantic transmission.** Input PCs are partitioned into discrete blocks, which are processed by a 3D convolution-based JCM network to extract spatial features, compress redundant data, and encode these features into DTCA symbols for transmission over the HCF channel. At the receiver, a JDD network employs 3D deconvolution to perform the inverse operations of the JCM network, decompressing the data, restoring the extracted spatial features, and merging the PC blocks to reconstruct the original PCs. See Fig. S1 (Supplementary Information) for the detailed network architecture and parameterization. In this semantic transmission scheme, conventional carrier phase recovery DSP algorithms (e.g., blind phase search and Viterbi–Viterbi) are ineffective. By contrast, comb line locking is modulation format-independent and effectively addresses the phase error issue.

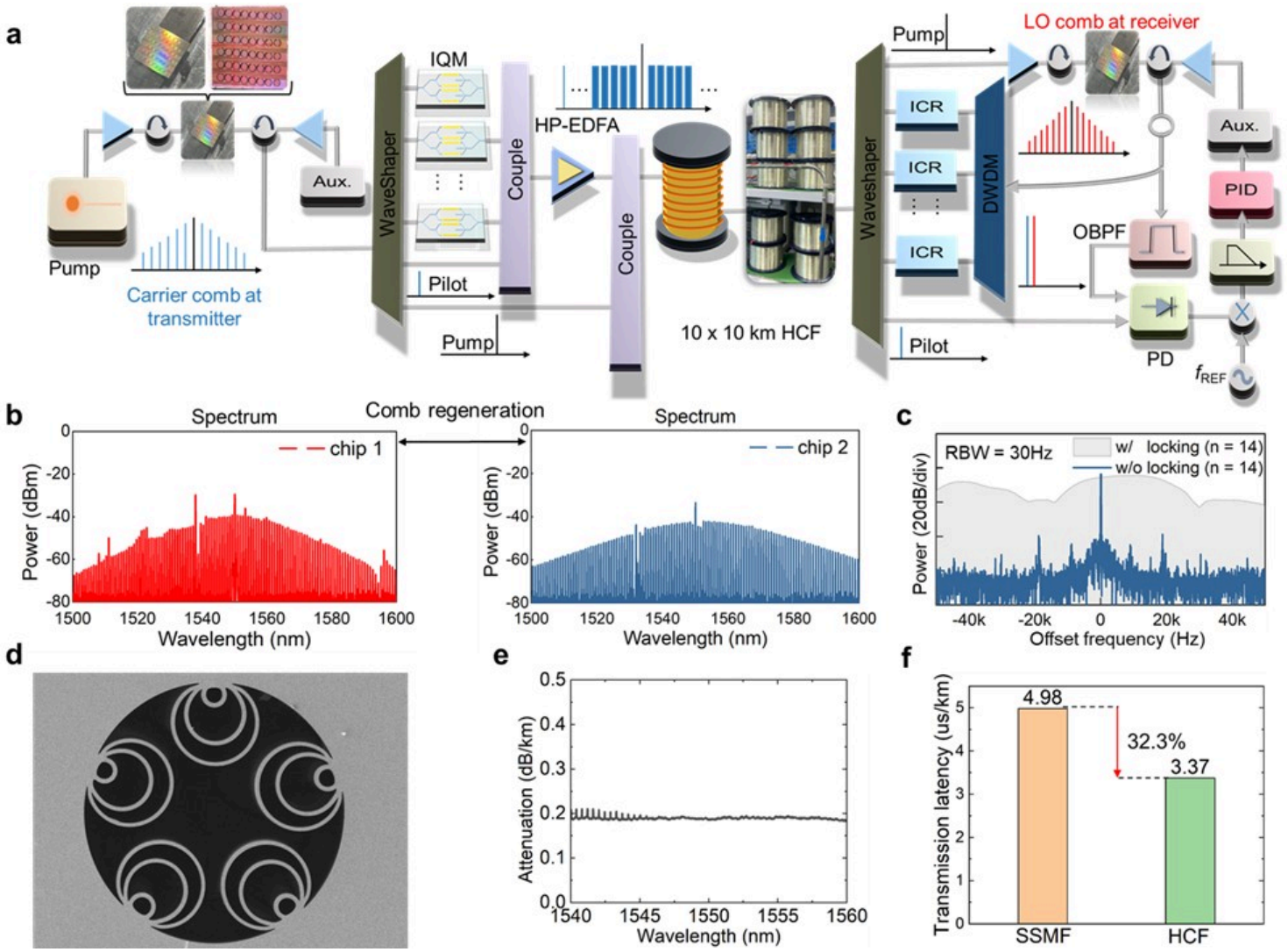
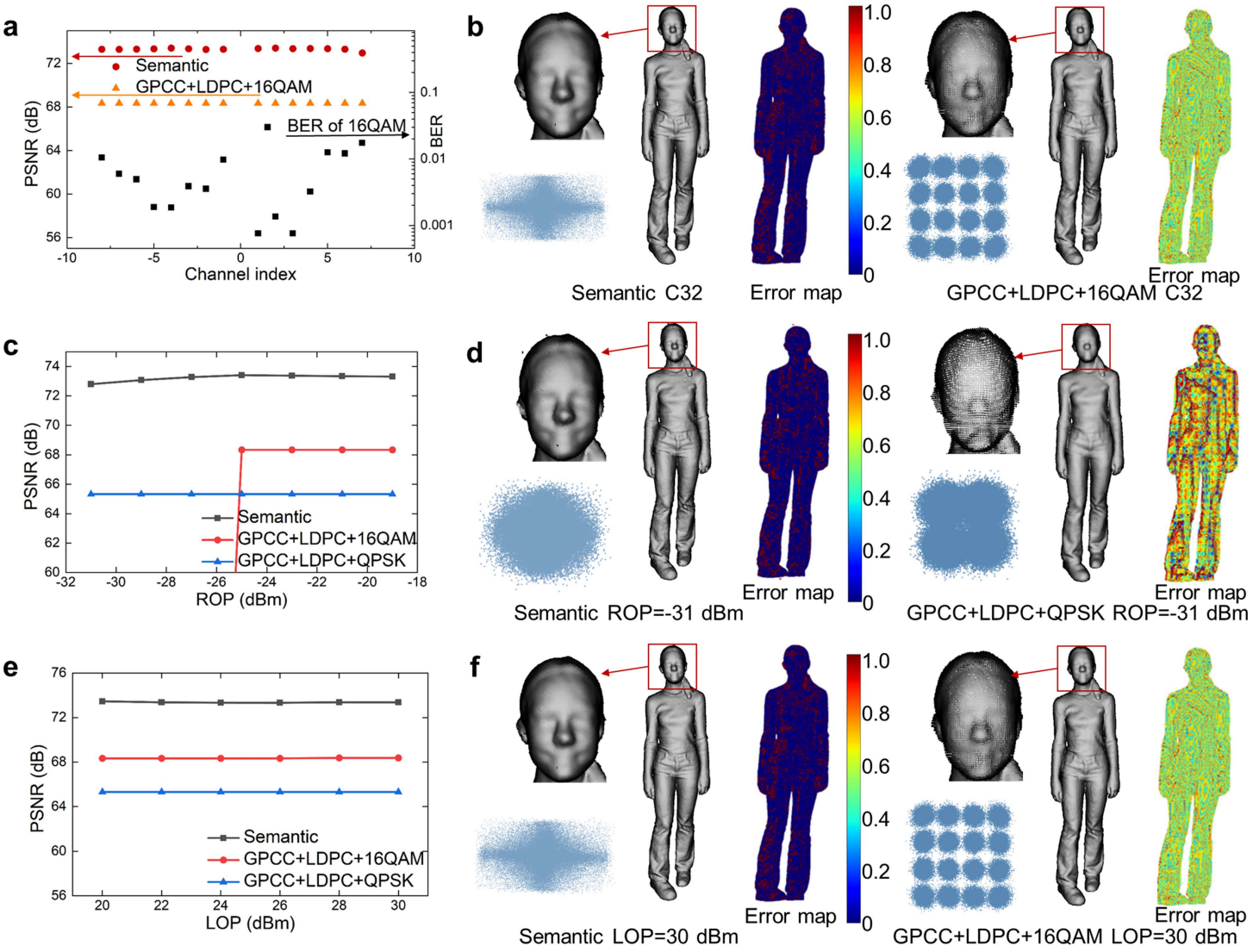



**Figure 3**

**Physical Link Setup, Optical Comb Performance, and HCF Characteristics.** (a) Experimental setup used for optical coherent transmission. On the transmitter side, an optical frequency comb is generated. The 15 data carriers, along with the pilot and pump, are selected using a waveshaper. The 15 data carriers are also subjected to IQ modulators through which 30 Gbaud single-polarization data are encoded onto the comb lines. The 15 channel signals and pilot are then amplified and coupled to the pump. The coupled optical signals are ultimately transmitted through a 100 km HCF. On the receiver side, the signal channels, pilot, and pump are separated by a waveshaper. The local oscillator comb is regenerated by the pump and locked to the combs on the transmitter side by the pilot, which are then used as local oscillators to enable coherent data reception. (b) Optical spectra of the carrier and regenerated local oscillator comb lines. (c) Phase noise performance of the system with and without two-point locking. (d) Cross-section of the HCF. (e) measured loss spectrum of the HCF. (f) Transmission latencies of HCFs and SSMFs. ICR, integrated coherent receiver; PID, proportional integral derivative; OBPF, optical band pass filter; Aux., auxiliary laser; PD, photodetector; IQM, IQ modulator; HP-EDFA, high-power erbium doped fiber amplifier.




## Figure 4

**Experimental results for 15-channel holographic transmission.** (a) Transmission results for 15 channels, including the BER for 16-QAM transmission and the PC transmission PSNR for both digital and semantic schemes. (b) Visual results for both semantic and 16-QAM transmission schemes in channel C32, including constellation maps, received PCs, and error maps. The error maps are calculated based on the point-to-point distance[57]. The color in the figure represents the point-to-point distance between the reconstructed PC and the ground truth PC. (c) PSNR of the transmitted PC versus different ROPs. (d) Visual results for both the semantic and QPSK transmission schemes when the ROP is − 31 dBm. (e) PSNR of the transmitted PC versus different LOPs. (f) Visual results for the semantic and 16-QAM transmission schemes when the LOP is 30 dBm.

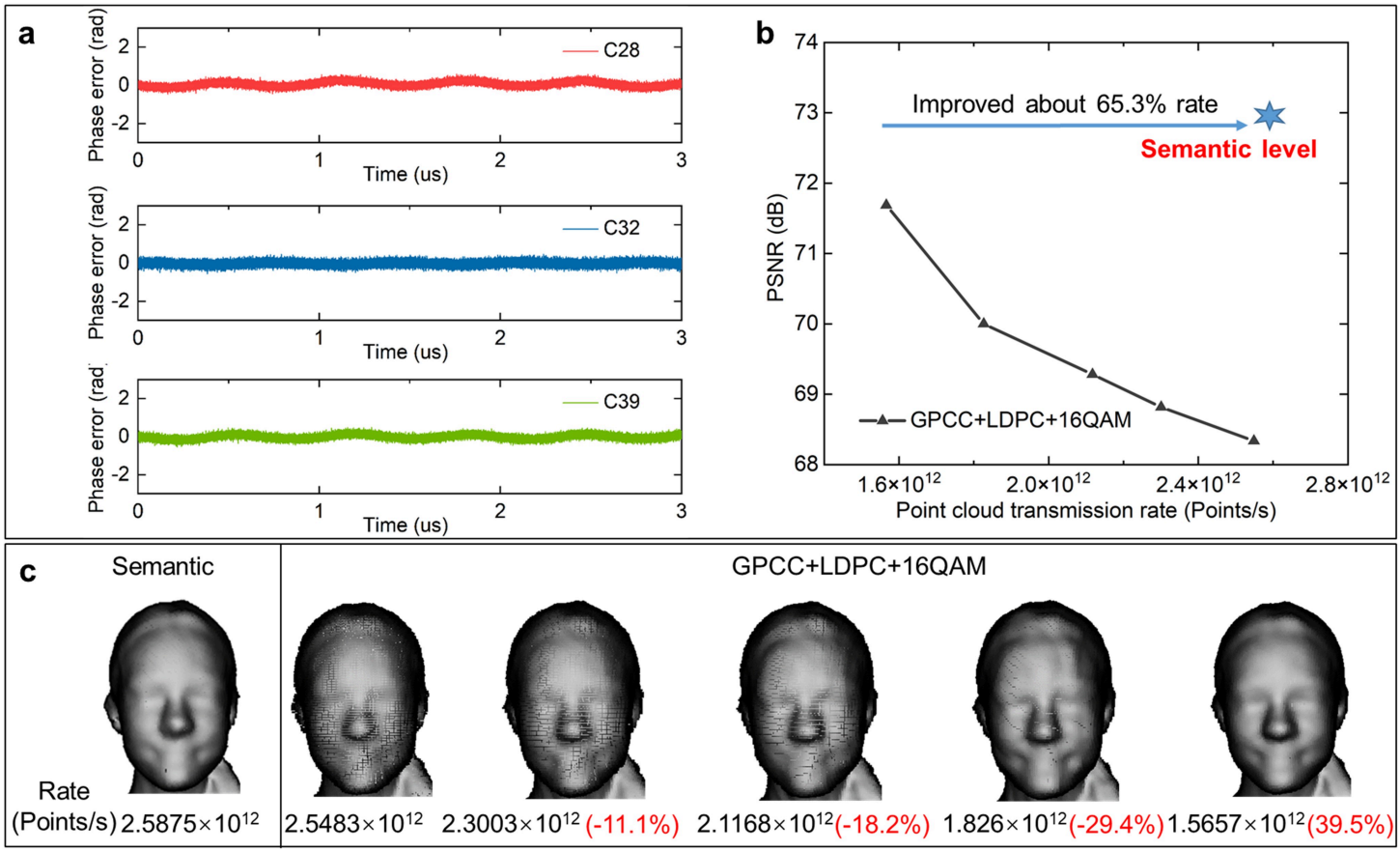



**Figure 5**

**Transmission performance analysis.** (a) Variation in system phase noise over time. (b) Relationship between different PC transmission rates and PSNR for 16-QAM transmission. (c) Visual comparison of the results of the semantic scheme and the 16-QAM transmission scheme at different transmission rates.

## Supplementary Files

This is a list of supplementary files associated with this preprint. Click to download.

- supportinformation.docx